Chemical Science

EDGE ARTICLE

Photocontrol of dynein motor activities by photoswitchable ATP antagonists

Received 00th January 20xx,
Accepted 00th January 20xx

DOI: 10.1039/x0xx00000x

www.rsc.org/

Sampreeth Thayyil,[a,b,#1] Yukinori Nishigami,[a,b,#1] Md. Jahirul Islam,[a,b,#2] P.K. Hashim,[a,b] Ken'ya Furuta,[c] Kazuhiro Oiwa,[c] Jian Yu,[d] Min Yao,[d] Toshiyuki Nakagaki,[a,b] Nobuyuki Tamaoki[a,b]*

Adenosine triphosphate (ATP) is the energy source for various biochemical processes and biomolecular motors in living things. Development of ATP antagonists and their stimuli-controlled actions offer a novel approach to regulate biological processes. Herein, we developed azobenzene-based photoswitchable ATP antagonists for controlling the activity of motor proteins; cytoplasmic and axonemal dyneins. The new ATP antagonsits showed reversible photoswitching of cytoplasmic dynein activity in an *in vitro* dynein-microtubule system due to the *trans* and *cis* photoisomerization of their azobenzene segment. Importantly, our ATP antagonists reversibly regulated the axonemal dynein motor activity for the force generation in a demembranated model of *Chlamydomonas reinhardtii*. We found that the *trans* and *cis* isomers of ATP antagonists significantly differ in their affinity to the ATP binding site.

Introduction

ATP, the "high energy molecule" is essential for all of the living things.[1] In biology, the energy released by ATP hydrolysis is supplied for synthesizing biomacromolecules, various cellular functions, muscle contraction, blood circulation, extracellular signaling, cargo transportation and locomotion of microorganism. [2–4] For instance, motor proteins such as kinesin, myosin and dynein utilize chemical energy from ATP hydrolysis to generate mechanical motion as a prerequisite for various cellular tasks.[5] Due to consumption at a high rate in diseased site such as tumor microenvironment, ATP is also considered as one of the possible targets for cancer therapy.[6,7] Hence, the development of molecular entities that can work as "ATP antagonist" has enormous possibilities in controlling the biochemical processes as well as in designing drugs. Additionally, by appending a stimuli-responsive motif to such ATP antagonist can potentially leads to the regulation of biological processes in a spatiotemporal manner. However, molecules that satisfy structural similarity to ATP together with stimuli-responsivity is extremely challenging to design.

Herein we show azobenzene-based ATP antagonists that respond to light irradiation via *trans* to *cis* isomerization reversibly.[8–14] The ATP antagonist binds to the receptor only in one of the isomer states (*trans*), thus can function as photoswitchable ATP antagonist. We demonstrate biological significance of photoswitchable ATP antagonists using dynein motor protein. Dynein is a cytoskeletal motor protein forming a large complex of 1-2 MDa and exists in two isoforms: cytoplasmic and axonemal dyneins.[15–17] There are multiple ATP

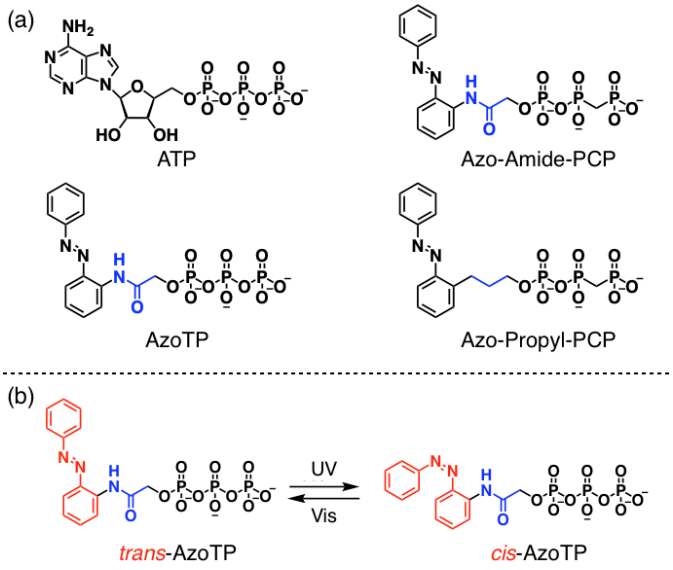

Fig. 1 (a) Molecular structures of ATP and ATP antagonists, AzoTP, Azo-Amide-PCP and Azo-Propyl-PCP. (b) Scheme showing the *trans* to *cis* isomerization of AzoTP by UV and Vis light irradiations.

[a] Research Institute for Electronic Science, Hokkaido University, Kita20, Nishi 10, Kita-ku, Sapporo, Hokkaido, 001-0020, Japan.
[b] Graduate School of Life Science, Hokkaido University, Kita 10, Nishi 8, Kita-ku, Sapporo, Hokkaido, 060-0810, Japan.
[c] Advanced ICT Research Institute, National Institute of Information and Communications Technology, Kobe, Hyogo, 651-2492, Japan.
[d] Faculty of Advanced Life Science, Hokkaido University, North 10 West 8, Kita-ku, Sapporo, Hokkaido 060-0810, Japan
[#1] These authors contributed equally to this work.
[#2] Current Address: Institute of Science and Technology Austria, A-3400 Klosterneuburg, Austria
E-mail: tamaoki@es.hokudai.ac.jp
Electronic Supplementary Information (ESI) available:]
See DOI: 10.1039/x0xx00000x

binding sites in dynein and the hydrolysis of bound ATP can induce mechanical stepping motion towards the minus-end of microtubules.[18–20] Utilizing ATP energy, cytoplasmic dynein transports intracellular cargos,[21, 22] while axonemal dynein drives the beating motion of flagella and cilia.[23, 24] With our photoswitchable ATP antagonist, we show an unprecedented photocontrol of both cytoplasmic and axonemal dyneins using a dynein-microtubule system and a demembranated *Chlamydomonas reinhardtii* model, respectively.

Results and discussion

We synthesized photoresponsive ATP antagonists (Figure 1a), AzoTP, Azo-Amide-PCP and Azo-Propyl-PCP according to the procedures described in the Supplementary Information and characterized unambiguously using a variety of analytical methods (HPLC, NMR, Mass) Figure S1, S10–S16. AzoTP, a hydrolysable analogue of ATP, has previously shown to power kinesin and myosin motor proteins in a photoswitchable manner.[25–27] Azo-Amide-PCP and Azo-Propyl-PCP with "amide" and "propyl" spacer between azobenzene (Azo) and methylene diphosphate (PCP) moieties were newly designed non-hydrolysable analogues of ATP. Photoswitching ability of ATP antagonists was studied by using absorption spectroscopy in BRB80 buffer (pH 6.9) (Figure 2).[28,29] As synthesized *trans* isomers of these ATP antagonists exhibited two absorption bands (λ_{max} = ~327 nm and 430 nm) assignable for π-π* and n-π* electronic transitions, respectively. Upon 365 nm light irradiation, the intensity of absorption bands was significantly altered to reach a UV photostationary state (UV_{PSS}) (Figure 2) containing 92% (Azo-Amide-PCP) and 88% (Azo-Propyl-PCP) *cis* isomer (determined by ^{1}H NMR in Figure S2 and Table S1). Upon 430 nm light irradiation (Vis_{PSS}), an opposite trend in the change of absorption bands containing 72% (Azo-Amide-PCP) and 75% (Azo-Propyl-PCP) *trans* isomer was observed. As shown in Figure 2b, d, the compounds (Azo-Amide-PCP and Azo-Propyl-PCP) underwent reversible *trans-cis* photoisomerization for many cycles without any fatigue. Thermal relaxation lifetimes for *cis* isomers in the compounds were >3 days at 25 °C (Figure S3).

Next, we investigated the effect of the compounds in the biological activity of dynein motor using an *in vitro* microtubule gliding assay in a flow cell. In this method, we used a fluorescently labelled (ATTO-647N) microtubules to visualize (excitation at 633nm and the emission maximum at 669nm) their gliding motility on cytoplasmic dynein (single motor unit)-coated glass surface. In sharp contrast to our previous observation of AzoTP-triggered gliding motion of microtubules or actin filaments on kinesin or myosin filaments-coated glass surface, respectively, AzoTP did not trigger microtubule gliding motion with dynein (Figure S4 and Movie S1). Even after UV (360 nm)/ Vis (430 nm) light irradiations to the flow cell containing dynein and AzoTP, we did not see any gliding motion of microtubules. These results indicate that dynein behaves differently towards AzoTP-powered filament motion compared to kinesin and myosin, presumably due to the complex structure and powering mechanism of dynein. To check the inhibitory behavior of AzoTP, we performed the microtubule gliding assay

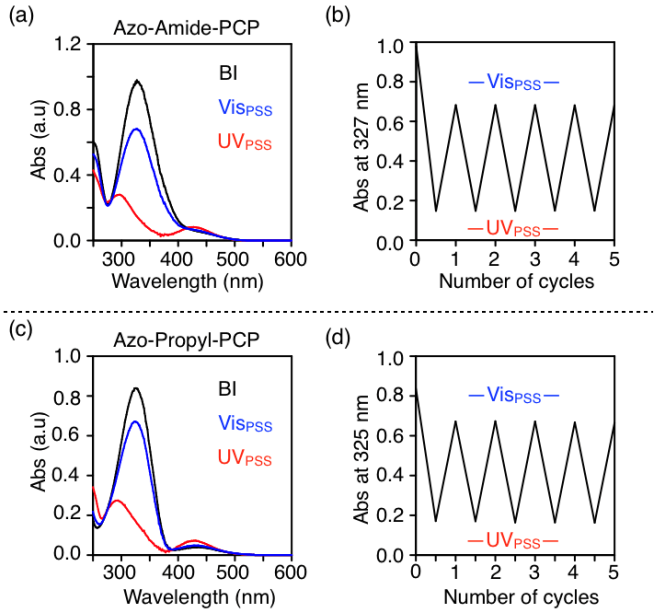

Fig. 2 UV-Visible absorption spectra of Azo-Amide-PCP (6.1 x10^{-4} M) (a) and Azo-Propyl-PCP (5 x 10^{-4} M) (c) in BRB-80 buffer at 25 °C before irradiation (BI, black line), photo-stationary state of UV (UV_{PSS}, red line) and Vis (Vis_{PSS}, blue line) irradiations. Absorbance changes at λ_{max} obtained by repeated irradiation (5 cycles) at UV_{PSS} and Vis_{PSS} (c and d).

in a flow cell containing dynein, ATP (0.1 mM) and varying amounts of AzoTP (0–10 mM). In this case, ATP in the system can drive the microtubule gliding motion, however we observed a significantly decreased gliding velocity upon increasing the amount of AzoTP (Figure 3a–c). For instance, the gliding velocity at 5 mM of AzoTP (0.02 μm s^{-1}) was ~20-times lower than that of without AzoTP (0.39 μm s^{-1}). K_i value obtained by fitting the experimental data using Michaelis-Menten equation assuming the competitive inhibition of AzoTP was 531 μM. Then we examined the photoinduced isomerization of AzoTP on the microtubule gliding velocity. Figure 3b shows the fluorescence images of gliding microtubule at 0 and 60 s before and after UV/ Vis light irradiations (Movie S2). At UV_{PSS}, the microtubule gliding velocity was 6.5-times higher (0.13 μm s^{-1}) than that of before irradiation (0.02 μm s^{-1}). At Vis_{PSS}, the gliding velocity became similar to that of before irradiation.

We also checked the ATP hydrolysis activity of dynein using enzyme linked inorganic phosphate assay. In this assay, the absorbance at 360 nm is directly proportional to inorganic phosphate released as a result of ATP hydrolysis (Figure S5). Interestingly, in the presence of dynein, AzoTP (100 μM) exhibited a higher rate of phosphate release (AzoTP: K_m = 65 μM, V_{max} = 3.4 s^{-1}) compared to ATP (100 μM) (K_m = 1.91 μM, V_{max} = 0.32 s^{-1})[30] (Figure S6) in a concentration dependent manner (Figure 3d). These results of the motility and hydrolysis experiments suggest that AzoTP occupy the recognition site for ATP in dynein in a competitive manner and capable of undergoing hydrolysis, however the hydrolysis reaction was uncoupled with the motility.[31] Such function as an antagonist

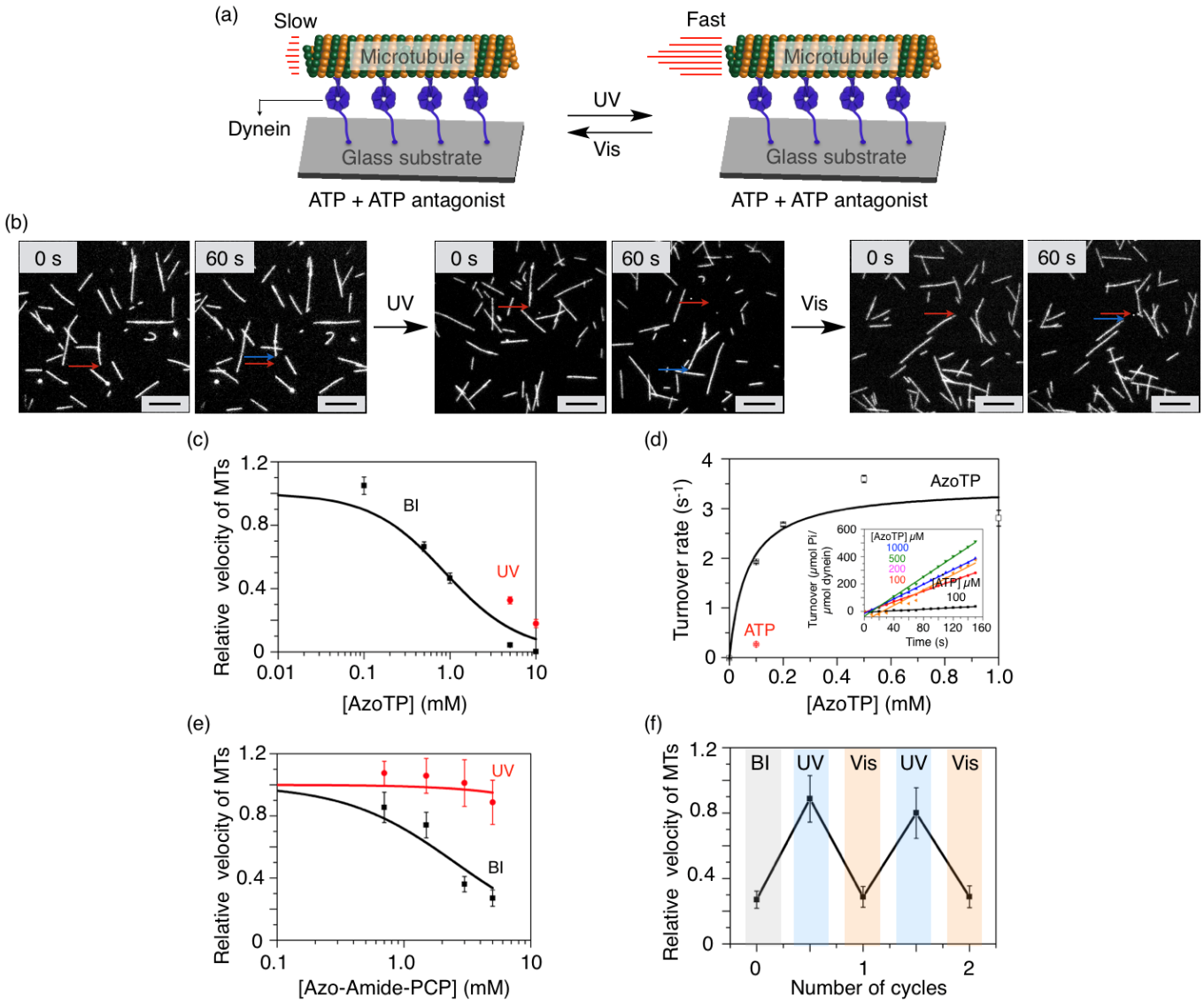

Fig. 3 Schematic representation of the dynein-driven microtubule motility on a glass substrate in the presence of ATP and ATP antagonists (a). Florescence microscopy images of the microtubules obtained at 0 s and 60 s after UV and Vis irradiations (AzoTP) Scale bars: 10 μm Red and blue arrows indicate the position of the same microtubule at 0 s and 60 s, respectively (b). Relative gliding velocity of microtubules (MTs) before and after UV/Vis light irradiations in the presence of AzoTP. Error bars represent the standard deviation of 10 microtubules in a single flow cell (c). Turnover of phosphate (Pi) release due to ATP or AzoTP hydrolysis by dynein at time 0–160 s (inset). Error bars represent the standard error (d). Relative gliding velocity of microtubules (MTs) before and after UV/Vis light irradiations in the presence of Azo-Amide-PCP. Error bars represent the standard deviation of 10 microtubules in a single flow cell (e). Reversible switching in the velocity of MTs over 2 cycles of Azo-Amide-PCP (5 mM; [ATP] = 50 μM) treated sample before (BI) and after UV/Vis light irradiations (f).

against ATP is intrinsically different depending on *trans* and *cis* isomers of AzoTP. Similar photoswitchable inhibitory behavior was also observed when we use Azo-Amide-PCP in the presence of ATP (50 μM) (Figure 3e) (K_i = 1.9 mM). Alternate UV and Vis irradiations were resulted in the reversible switching of microtubule gliding velocity (Figure 3f and Movie S3).

We then investigated the effect of ATP antagonists for the control of dynein motor activity in a eukaryotic organism. *Chlamydomonas reinhardtii* is a biflagellar single-cell green algae having dynein motors at its outer and inner arms of the flagella. In *C. reinhardtii*, a cooperative action of multiple dynein motors triggered by ATP produces propulsive force for the beating motion of its flagella.[32-34] We used a uniflagellar mutants of *C. reinhardtii*, which is known to undergo rotational motion.[35–36] To study the effects of ATP antagonists on the behavior of *C. reinhardtii*, the demembranated model was prepared according to the previous studies. [37] We first treated *C. reinhardtii* with a detergent solution to remove its cell membrane, transferred to reactivation buffer containing ATP and observed under an inverted microscope. The resulting demembranated cell exhibited active rotational motion in the presence of ATP (Figure S7). However, the rotational motion

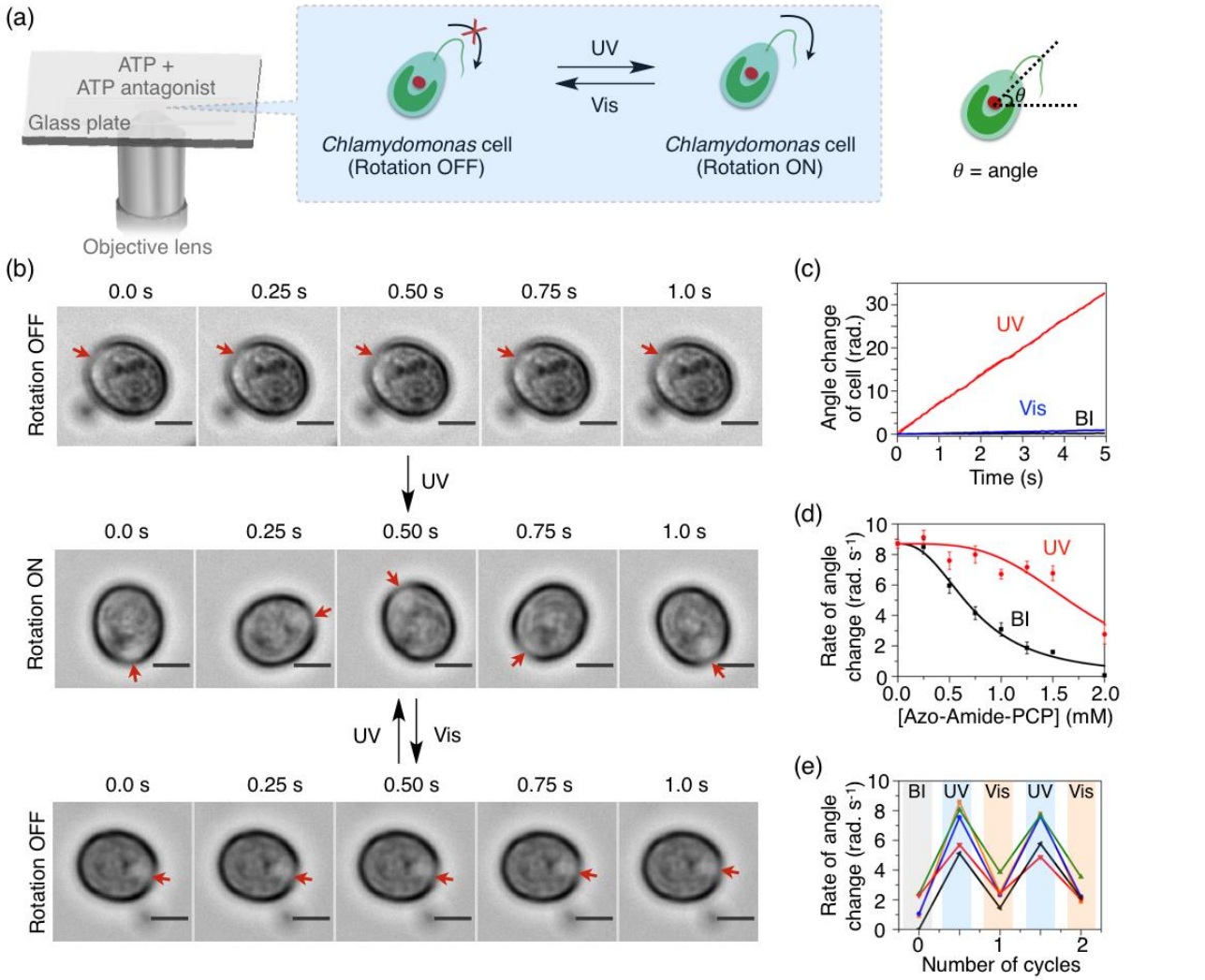

Fig. 4 Simplified scheme of experimental condition used for the microscopy imaging of a mutated *Chlamydomonas* cell before and after UV/Vis light irradiations (a). Optical microscopy images showing the rotational motion of the *Chlamydomonas* cell at time 0–1.0 s before and after UV (5 s)/Vis (7 s) light irradiations to the chamber containing Azo-Amide-PCP (1.25 mM) and ATP (100 μM) (b). Scale bars: 5 μm. (red arrows head indicate the reference point of the cell rotation). Graph showing the angle change of *Chlamydomonas* cell at time 0–5 s (c), the rate of angle change of the cell with different concentrations of Azo-Amide-PCP (d), and the reversible switching in the rate of angle change of 5 different cells (black, red, blue, orange and green lines) over 2 cycles before (BI) and after UV/Vis light irradiations (e). Error bars represent the standard error of 8–10 *Chlamydomonas*.

was inhibited when ATP antagonist (Azo-Amide-PCP or Azo-Propyl-PCP) present in the reactivation solution (Figure 4 and Figure S8). Interestingly, the rotational motion of *Chlamydomonas* cell restarted after direct UV irradiation (360 nm, 5 s) to the experimental system. Subsequent Vis irradiation (430 nm, 7 s) inhibited the rotational motion cell again (see microscopy images in Figure 4a). We measured the angle change with respect to the center of the rotating cell and found a significant difference in the values before (0.03 rad. s^{-1}) and after UV irradiation (6.53 rad. s^{-1}) (Azo-Amide-PCP) (Figure 4c). The rate again decreased significantly after Vis irradiation (0.19 rad. s^{-1}). We optimized the concentration of Azo-Amide-PCP that show maximum inhibition (99% at 1.25 mM) of the cell rotation with reversible photoswitching characteristics (Figure 4d,e, movie S5 and S7). Similar reversible switching of the rate of angle change was also observed in the case of Azo-Propyl-PCP (BI; 0.01 rad. s^{-1}, UV; 5.07 rad. s^{-1} and Vis (0.71 rad. s^{-1}) (Figure S8 and movie S4 and S6). We checked the effect of UV/Vis irradiations for the rotational motion of cell without ATP antagonists and found no inhibitory behavior (Figure S7). These results indicate that ATP antagonist present in the experimental system plays an important role for the reversible inhibition of *Chlamydomonas* cell rotation, presumably via binding with axonemal dyneins. The K_i values obtained by fitting the experimental data of Azo-Amide-PCP were 0.27 mM (*trans*) and 4.73 mM (*cis*) while those of Azo-Propyl-PCP were 0.03 mM (*trans*) and 0.36 mM (*cis*). The difference in K_i values between *trans* and *cis* isomers of ATP antagonists further indicates that

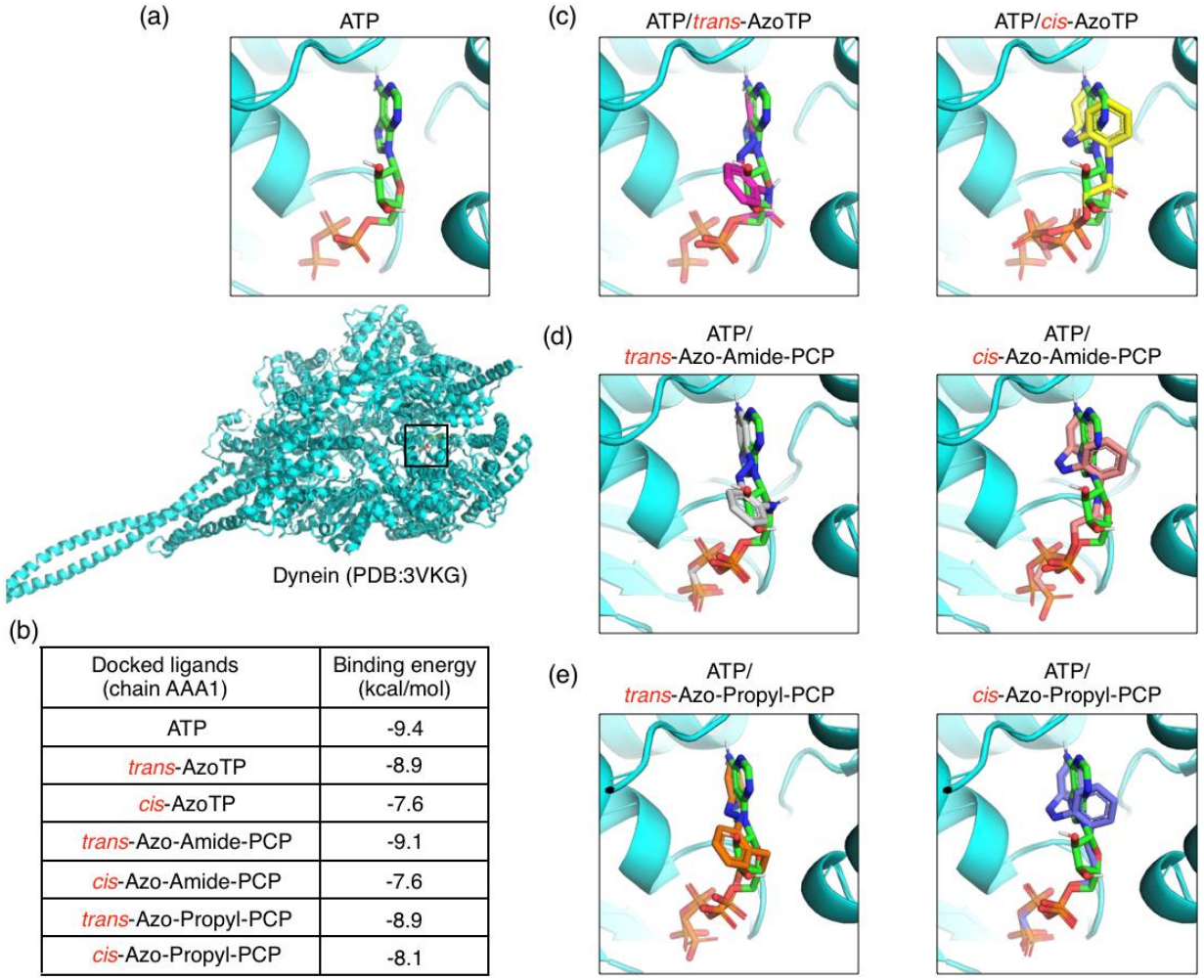

(b)

Docked ligands (chain AAA1)	Binding energy (kcal/mol)
ATP	-9.4
trans-AzoTP	-8.9
cis-AzoTP	-7.6
trans-Azo-Amide-PCP	-9.1
cis-Azo-Amide-PCP	-7.6
trans-Azo-Propyl-PCP	-8.9
cis-Azo-Propyl-PCP	-8.1

Fig. 5 Scheme showing the docked ligands in the ATP binding site of cytoplasmic dynein (AAA1 chain; PDB 3VKG) (a). Table showing the binding energy of docked ligands (b). The ligand ATP in the binding site of dynein AAA1 chain superimposed with the docked *trans*/*cis*-AzoTP (c), *trans*/*cis*-Azo-Amide-PCP (d) and *trans*/*cis*-Azo-Propyl-PCP (e).

the ATP antagonists preferably bind to dynein in *trans* isomer than their *cis* isomer.

We studied molecular docking to know the ATP antagonist binding with the receptors of dynein using AutoDock Vina. The cytoplasmic dynein protein structure from protein data bank (3VKG) was used as the ATP receptor model.[38] Figure 5 shows the docked ligands in the ATP binding site of dynein (AAA1 chain) superimposed with the docked *trans*/*cis*-AzoTP and *trans*/*cis*-Azo-Amide-PCP. Azobenzene motif of the ATP antagonists in its *trans* isomer showed a parallel orientation with the adenine motif of ATP, however *cis* isomer was in perpendicular orientation (Figure S9). This result indicates the shape incompatibility of ATP antagonist in their *cis* isomer. Binding affinity of *trans* and *cis* isomers docked ATP antagonist further indicate the less affinity of *cis* isomers to the binding site than *trans* isomers (Figure 5b).

Conclusions

In conclusion, we successfully developed azobenzene-based ATP antagonists that show a reversible control of motor activity of isolated cytoplasmic dynein as well as axonemal dynein of a eukaryotic organism. Using an *in vitro* microtubule motility assay, we demonstrated that the ATP antagonists can inhibit the gliding motion of microtubule, however, regain the motion by UV light irradiation. The reversible photoisomerization of ATP antagonists between *trans* and *cis* isomers lead the reversible photoswitching of the microtubule gliding motility. Our ATP antagonists also showed the inhibition of the axonemal dynein activity for force generation in a demembranated model of *Chlamydomonas reinhardtii*. The rotational motion of *Chlamydomonas* cell was inhibited in the presence of ATP antagonists, however reverted rapidly by UV irradiation, and alternate UV/Vis irradiations resulted in the reversible switching of the rotational motion of *Chlamydomonas* cell. We also found that the *trans* and *cis* isomers of ATP antagonists significantly differ in their affinity to the ATP binding site of cytoplasmic dynein. Our data show the power of a reversible photoregulatory tool in controlling the function of biological

motor in a dynamic manner. Taking advantage of the high spatiotemporal precision of photochromic system, the interesting next step is to apply our ATP antagonists for specific macroscopic function in living animal.

Methods

General procedure for the synthesis of AzoTP derivatives

The AzoTP derivatives were synthesized according to our previous reports up to the monophosphate-tethered azobenzene and with a slight modification in the final methylene diphosphate attachment.[25–27] (See ESI for details)

Preparation of recombinant human cytoplasmic dyneins

The recombinant human cytoplasmic dynein construct (monomeric) was prepared as His8-SBP-FLAG-BioEase-DHC1(1306–4646) in the pcDNA3.4 plasmid vector.[30] The construct was transiently expressed in the Expi293 cells, purified via two-step affinity chromatography using Ni-IMAC resin (156–0133, Bio-Rad), and anti-FLAG agarose (A2220, Sigma-Aldrich).

Preparation of tubulin and fluorescently labelled microtubules

Tubulin was prepared according to the methods described previously.[40] Briefly, tubulin was purified from porcine brain through two successive cycles of polymerization and depolymerization using a high molarity PIPES buffer method. An aliquot of tubulin was labelled with ATTO 647N NHS ester (AD 647N-31, ATTO-TEC). The yield of the labelling was ca. 19%. To prepare fluorescently labelled microtubules, ATTO 647-tubulins were copolymerized with unlabeled tubulin at a ratio of 1:5 for 30 min at 37 ℃ in the presence of 1mM GTP in BRB80 (80 mM PIPES-KOH pH 6.8, 1 mM EGTA, and 1 mM $MgCl_2$) and stabilized with 40 μM paclitaxel (T1912, Sigma-Aldrich).

Dynein-microtubule *in vitro* motility assay

Microtubule gliding on cytoplasmic dynein-coated surface was observed in the presence of ATP and various ATP antagonists at 24 ± 1 °C, according to the method described previously with slight modifications.[39] The space formed between two coverslips (18 × 18 mm^2 #C218181 and 24 × 32 mm^2 #MGCS001E7, thickness No.1; Matsunami Glass) with the spacer of two slivers of Parafilm (Heathrow Scientific LLC) was used as a flow cell.[40] Heating the flow cell at 100 °C on the hot plate for few seconds melted the Parafilm and the film sealed tightly the coverslips together. The resultant flow cell has approximate dimensions of 2.5 mm in width, 18 mm in length and 150 μm in height.

The flow cell was filled with 7 μL of 2 mg/mL biotinylated BSA (A6043, Sigma-Aldrich) in BRB80 buffer and incubated for 3 min at room temperature. The flow cell was washed with 35 μL of BRB80 buffer and then incubated with 7 μL of 1 mg/mL streptavidin (Type II, 192–11641, Wako; filtered with a 0.1 μm spin filter before use) in 10 mM PIPES-KOH pH 6.8. After 3-minute incubation, the flow cell was filled with 21 μL of 7 mg/mL casein (07319-82, Nacalai) in casein buffer (25 mM HEPES-NaOH, pH 8.6, 50 mM K-acetate) and incubated for 3 min at room temperature. The flow chamber then was filled with 7 μL of 45 μg/mL dynein construct in buffer A (25 mM imidazole pH 8.0, 25 mM KCl, and 4 mM $MgCl_2$) for 3 min at room temperature. After washing with 21 μL of buffer A, 21 μL of Gliding buffer (25 mM imidazole pH 8.0, 25 mM KCl, 6 mM $MgCl_2$, 0.7 mg/mL casein, 100 μM ATP, 0.218 mg/mL glucose oxidase, 0.04 mg/mL catalase, 2 mM dithiothreitol, 10 μM paclitaxel, and 25 mM glucose) including ca. 4 μg/mL fluorescent microtubules was introduced into the flow cell and then washed with Gliding buffer without microtubules. Microtubule gliding was imaged using a custom-built, objective-type total internal reflection fluorescence microscope based on Ti-E (Nikkon) equipped with an oil immersion objective lens (CFI Apochromat TIRF 60XC Oil, NA/1.49). The fluorescence dye was excited using a 632.8-nm He-Ne laser (Model 30991, 5 mW, Research Electro Optics Inc.). A dichroic mirror (FF640-FDi01-25x36, Semrock) and a bandpass filter (FF01-676/29, Semrock) were used. The fluorescence image was detected by an EMCCD camera (iXon Life 897, Andor). The following equation was used for fitting (K_m value of ATP[41] = 152 ± 18 μM, [S] = 50 or 100 μM).

$$v = (K_m + [S])/(K_m(1 + [I]/K_i) + [S]).$$

Relative velocity $= v/v_0$, where v_0 is the velocity in the absence of an inhibitor.

Measurement of steady-state ATPase

Steady-state ATPase activities of dynein in the presence of ATP antagonists were measured using the EnzChek Phosphate Assay Kit (Thermo Fisher Scientific). The absorbance at 360 nm was monitored by the SYNERGY H1 microplate reader (BioTEK) every 10 s for 10 min at 25°C. Assays were performed in reaction buffer (10 mM PIPES-KOH at pH 6.8, 25 mM potassium acetate, 4 mM $MgSO_4$, 1 mM EGTA, 20 μM taxol, 200 μM 2-amino-6-mercapto-7-methylpurine riboside and 1 U/ml purine nucleoside phosphorylase) containing 100 nM dynein and 100 μM ATP, or various concentrations of antagonists (0.1-1 mM).

Cell culture

Chlamydomonas reinhardtii strain uni-1, was grown in TAP medium at 25° C in light/dark cycles (12 h /12 h).[37] 15 ml of cell suspension in the mid-log phase was centrifuged at 1000 × g for 3 min. The obtained cell pellet was washed twice with Milli Q and a wash buffer (10 mM HEPES, 0.5 mM EGTA, pH 7.4). For demembranation, 0.25 mL (5 volume of cell pellet) of an ice-chilled aqueous solution (30 mM HEPES, 5 mM $MgSO_4$, 1 mM DTT, 1 mM EGTA, 50 mM K-acetate, 1% (w/v) polyethylene glycol [20,000 mol wt] and 0.1 % (v/v) Nonidet P-40) was added to the cell pellet and incubated for 5 min at 25°C. The suspension was gently mixed to avoid flagella loss. Then, 10 μL of demembranated cells suspension was diluted with 200 μL of the above aqueous solution. For reactivation, 10 μL of the diluted solution was mixed with 10 μL of reactivation solution with 200 μM ATP. All the experiments after demembranation were performed at 0° C except for the microscopic observation.

Microscopic observation of the cell rotation

The plasma-treated cover glass (Matsunami no.1, 24x50 mm) was coated with 20 μL of 2% (w/v) MPC polymer (Lipidure-CM5206; NOF Corporation) in ethanol. The cover glass was heated at 50° C for 30 min to dry ethanol. The observation solution containing the demembranated cells was placed into a chamber made by a silicone sheet (thickness of 1 mm) with a hole 4mm diameter sandwiched between the MPC coated glass and a cover glass (Matsunami no.1, 18x24 mm). The cells in the demineralized cell suspension placed in the holes of the silicon sheet were observed in red light (M700L4, 700nm; Thorlabs) under an inverted microscope (IX 73; Olympus) using an objective lens (LUCPlan 40x, NA 0.6; Olympus) equipped with a CMOS camera (ORCA-Flash4.0; Hamamatsu). The video recording speed was set to 20 FPS. Fiji (https://imagej.net/software/fiji/) was used to analyze the angle change of the cells at before and after irradiation of UV (365 nm)/Vis (430 nm) light. The cells ten seconds after/before irradiation were used for analysis. The movement of the cells for five seconds was used to obtain the angle change. The following equation was used for fitting the experimental data (see ESI for details).

$$v_{\mathrm{i}} = v_0\,(K_{\mathrm{m}} + [\mathrm{S}])/(K_{\mathrm{m}}(1 + [\mathrm{I}]^n/K_{\mathrm{i}}) + [\mathrm{S}])$$

Molecular docking

The binding site of ADP in chain A near to LEU1947 was chosen as the docking site. Only polar hydrogen atoms were added to the model, and then the input PDBQT file of the receptor was generated by using AutoDockTools (1.5.6).[42] The 3D models of all the ligands were generated with their SMILES strings by using eLBOW program in Phenix software suite.[43] Then, AutoDockTools merged the non-polar hydrogen atoms and set up the rotatable bonds to create the input PDBQT file of candidate ligands. A grid box with the size of (16 Å, 22 Å, 16 Å) centered at (x = 76 Å, y = 138 Å, z = 68Å) was set up for the docking simulation which was performed by using Autodock Vina(1.1.2).[44]

Conflicts of interest

There are no conflicts to declare.

Acknowledgements

This work was supported by KAKENHI Grants-in-Aid for Scientific Research B (18H02042 (NT)), and also partially by Grants-in-Aid for Transformative Research Areas (21H05308(YN), 21H05310 (TN)), Fostering Joint International Research (B) (19KK0180 (YN)) by the Cooperative Research Program of the Network Joint Research Center for Materials and Devices from the Ministry of Education, Culture, Sports, Science and Technology (MEXT) and the Dynamic Alliance for Open Innovation Bridging Human, Environment and Materials from MEXT. We thank Prof. Kamiya and Kato-Minoura (Chuo University), for providing *Chlamydomonas* reinhardtii strain uni-1

Notes and references

1 P. Mitchell, *Science,* 1979, **206**, 1148–1159
2 G.M Cooper, The cell: A molecular approach. 2nd edition, 2000, Sinauer Associates, Sunderland (MA).
3 M. Regnier, D.M Lee, and E. Homsher, *Biophys J.* 1998, **74**, 3044–3058.
4 M. Kinoshita, *Biophysics and Physicobiology,* 2021, **18**, 60–66.
5 R. D. Vale, *Cell*, 2003, **112**, 467–480.
6 H J Agteresch, P C Dagnelie, J W van den Berg, and J H Wilson, *Drugs*, 1999, **58**, 211–232.
7 S.M Gilbert, C.J Oliphant, S. Hassan, A.L Peille, P. Bronsert, S. Falzoni, F. Di Virgilio, S. McNulty, and R. Lara, *Oncogene*, 2019, **38**, 194–208.
8 I. M. Welleman, M. W. H. Hoorens, B. L. Feringa, H. H. Boersma and W. Szymanski. *Chem. Sci.*, 2020, **11**, 11672–11691.
9 A. A. Beharry and G. A. Woolley, *Chem. Soc. Rev.*, 2011, **40**, 4422–4437.
10 H. M. D. Bandara and S. C. Burdette, *Chem. Soc. Rev.*, 2012, **41**, 1809–1825.
11 T. Seki, *Bull. Chem. Soc. Jpn.*, 2018, **91**, 1026–1057.
12 M. Kathan and S. Hecht, *Chem. Soc. Rev.*, 2017, **46**, 5536–5550.
13 D. M. Barber, S. A. Liu, K. Gottschling, M. Sumser, M. Hollmann and D. Trauner, *Chem. Sci.*, 2017, **8**, 611–615.
14 M. Schehr, C. Ianes, J. Weisner, L. Heintze, M. P. Müller, C. Pichlo, J. Charl, E. Brunstein, J. Ewert, M. Lehr, U. Baumann, D. Rauh, U. Knippschild, C. Peifer and R. Herges, *Photochem. Photobiol. Sci.*, 2019, **18**, 1398–1407.
15 I. R. Gibbons, *Cell Motil. Cytoskeleton*, 1995, **32**, 136–144.
16 B. M. Paschal and R. B. Vallee, *Nature*, 1987, **330**, 181–183.
17 P. Höök and R. B. Vallee, *J. Cell Sci.*, 2006, **119**, 4369–4371
18 G. Bhabha, H. C. Cheng, N. Zhang, A. Moeller, M. Liao, J. A. Speir, Y. Cheng and R. D. Vale, *Cell*, 2014, **159**, 857–868.
19 T. Kon, M. Nishiura, R. Ohkura, Y. Y. Toyoshima and K. Sutoh, *Biochemistry*, 2004, **43**, 11266–11274.
20 T. Kon, T. Oyama, R. Shimo-Kon, K. Imamula, T. Shima, K. Sutoh and G. Kurisu, *Nature*, 2012, **484**, 345–350.
21 S. Karki and E. L. Holzbaur, *Curr. Opin. Cell Biol.*, 1999, **11**, 45–53.
22 R. B. Vallee, J. C. Williams, D. Varma and L. E. Barnhart, *J. Neurobiol.*, 2004, **58**, 189–200.
23 I. R. Gibbons *J. Cell Biol.*, 1981, **91**, 107–124.
24 L. M. DiBella and S. M. King, *Int. Rev. Cytol.*, 2001, **210**, 227–268.
25 N. Perur, M. Yahara, T. Kamei and N. Tamaoki, *Chem. Commun.*, 2013, **49**, 9935–9937.
26 H. M. Menezes, M. J. Islam, M. Takahashi and N. Tamaoki, *Org. Biomol. Chem.*, 2017, **15**, 8894–8903.
27 M. J. Islam, K. Matsuo, H. M. Menezes, M. Takahashi, H. Nakagawa, A. Kakugo, K. Sada and N. Tamaoki, *Org. Biomol. Chem.*, 2019, **17**, 53–65.
28 D. Samanta, J. Gemen, Z. Chu, Y. Diskin-Posner, L. J. W. Shimon and R. Klajn, *Proc. Natl. Acad. Sci. U. S. A.*, 2018, **115**, 9379–9384.
29 J. Volaric, W. Szymanski, N. A. Simeth, and B. L Feringa, *Chem. Soc. Rev.*, 2021, **50**, 12377–12449.
30 R. Ibusuki, T. Morishita, A. Furuta, S. Nakayama, M. Yoshio, H. Kojima, K. Oiwa, and K. Furuta. *Science*, 2022, in press.
31 T. Shimizu, *J. Biochem.*, 1987, **102**, 1159–1165.

32 O. Kagami and R. Kamiya, *J. Cell Sci.*, 1992, **103**, 653–664.
33 J. Lin and D. Nicastro. *Science* 2018, **360**, eaar1968.
34 S. Toba, H. Iwamoto, S. Kamimura and K. Oiwa, *Biophys. J.*, 2015, **108**, 2843–2853.
35 C.J. Brokaw, D.J.L. Luck, and B. Huang, *J. Cell Biol.*, 1982, **92**, 722–732.
36 Huang B, Ramanis Z, Dutcher SK, and Luck DJ, *Cell.,* 1982, **29**, 745-753.
37 R. Kamiya and G. B. Witman, *J. Cell Biol.*, 1984, **98**, 97–109.
38 T. Kon, T. Oyama, R. Shimo-Kon, K. Imamula, T. Shima, K. Sutoh, and G. Kurisu. *Nature*, 2012, **484**, 345–350.
39 A. Furuta, M. Amino, M. Yoshio, K. Oiwa, H. Kojima and K. Furuta. *Nat. Nanotechnol*, 2017, **12**, 233–237.
40 M. Castoldi, A. V. Popov. *Protein Expr. Purif.* 2003, **32**, 83–88.
41 T. Torisawa, M. Ichikawa, A. Furuta, K. Saito, K. Oiwa, H. Kojima, Y.Y. Toyoshima, K. Furuta. *Nat. Cell Biol*, 2014, **16**, 1118–1124.
42 G. M. Morris, R. Huey, W. Lindstrom, M. F. Sanner, R. K. Belew, D. S. Goodsell, and A. J. Olson. *J. Computational Chemistry*, 2009, **16**, 2785–2791.
43 P. D. Adams, P. V. Afonine, G. Bunkóczi, V. B. Chen, I. W. Davis, N. Echols, J. J. Headd, L.-W. Hung, G. J. Kapral, R. W. Grosse-Kunstleve, A. J. McCoy, N. W. Moriarty, R. Oeffner, R. J. Read, D. C. Richardson, J. S. Richardson, T. C. Terwilliger and P. H. Zwart. *Acta Cryst. D,* 2010, **66**, 213–221.
44 O. Trott and A. J. Olson. *Journal of Computational Chemistry* 2010, **31**, 455–461.

TOC